Boosting NO removal performance of selective catalytic reduction with NH_3 on hydrotalcite derived NiCuFe mixed oxides synthesized via urea hydrothermal method

Fan Yang[1] · Xinpeng Wang[1] · Chao Qu[1] · Fanwei Meng[1] · Wenyi Liu[1] · Qing Ye[1]

Abstract

NiCuFe layered double oxide (LDO) catalysts were synthesized using co-precipitation, impregnation, and urea hydrothermal methods. The NH_3-SCR activity of NiCuFe-LDO catalysts was investigated to determine the effect of different synthesis methods. All NiCuFe-LDO samples exhibited good catalytic performance at low temperatures, with the sample synthesized using the urea hydrothermal method (NiCuFe-LDO-3) being the most efficient catalyst. The NiCuFe-LDO-3 catalyst achieved over 80% NO conversion in the temperature range of 180 °C to 280 °C, with a peak of 95.13% at 240 °C. The physicochemical properties of the samples were systematically characterized using XRD, SEM, BET, NH_3-TPD, H_2-TPR, XPS, and in-situ DRIFTS. The results showed that the NiCuFe-LDO-3 sample had the best crystallinity, as demonstrated by XRD and SEM. BET analysis revealed that the NiCuFe-LDO-3 sample had the largest specific surface area. The NiCuFe-LDO-3 sample was found to have more acidic sites and a better redox capacity than the other samples, according to the H_2-TPR and NH_3-TPD results. In-situ DRIFTS analysis showed that the catalyst operates through both E–R and L–H reaction mechanisms.

Keywords NH_3-SCR · $NiCuFeO_x$ · LDO · Heterogeneous catalysis · Urea Hydrothermal

Introduction

Air quality is a pressing public concern, and nitrogen oxides (NO_x) are a major contributor to poor air quality [1]. Many associated environmental problems such as photochemical smog, haze, and acid rain have been caused by NO_x. Selective

---

✉ Qing Ye
yeqing@bjut.edu.cn

1 Key Laboratory of Beijing On Regional Air Pollution Control, Department of Environmental Science, College of Environmental Science & Engineering, Beijing University of Technology, Beijing 100124, China

catalytic reduction with NH_3 (NH_3-SCR) is widely recognized as the most effective technology for NO_x removal [2, 3]. In recent times, V_2O_5-WO_3/TiO_2 catalysts have shown remarkable NH_3-SCR reactivity, good SO_2 tolerance, and high catalytic performance between 300 and 400 °C [4]. However, some limitations include a narrow operating temperature range, inadequate selectivity towards N_2, and the bio-toxicity of vanadium limiting its application in NH_3-SCR [5]. Consequently, there is a need for a kind of no-toxicity catalyst with improvement in NH_3-SCR performance, particularly at low temperatures.

Iron-based zeolite catalysts have attracted substantial attention as possible NH_3-SCR catalyst candidates for diesel applications, owing to their effectiveness in reducing NO [6]. While iron-based zeolite catalysts demonstrate remarkable high-temperature activity, their low-temperature activity presents a constraining factor, as the adsorption of ammonia on the iron sites at low temperatures could impede the admission of NO_x molecules [7, 8]. In contrast to Fe-based catalysts, Cu-based catalysts have superior low-temperature activity, but do not benefit from higher temperatures due to the formation of unwanted products from the oxidation of NH_3 by O_2 [9]. Therefore, catalysts composed of Cu-Fe may present greater NO conversions across a wider temperature spectrum than individual catalysts due to their distinct characteristics. On the other hand, some other transition metal elements such as Ni have significant potential in NH_3-SCR reactions [10–12]. It is worth noting that these metals exhibit exceptional oxygen storage capacity and unique redox properties. For that, the activity of catalysts can be significantly improved by doping transition metals.

To combine the advantages of Cu, Fe, and other transition metal elements, a kind of composite metal oxide catalyst is needed. Layered double hydroxides (LDH) are plate-like ionic compounds that consist of positively charged hydro magnesite-like layers, anions, and solvated molecules in the interlayer region [13]. Highly dispersed layered double oxides (LDOs) can be produced by calcining LDHs, which have been widely researched for the application in NH_3-SCR. Wang et al. examined diverse LDO types and found that layered double oxides have superior performance to catalysts synthesized through traditional methods [14]. In addition, studies have reported that cation exchange can occur between metal ions and LDH [15]. Further studies have shown that cation exchange is more favorable under alkaline conditions [16]. The stratified arrangement of layered double oxides provides a broad specific surface area, creating extra binding sites for active components. This particular structure permits the highly dispersed organization of numerous active metal components, modifying the surface electronic features, and resulting in the creation of novel active catalytic sites.

In this work, NiCuFe-LDO catalysts were successfully synthesized by co-precipitation, impregnation, and urea hydrothermal methods for NO_x removal. The effects of the three synthesizing methods of Ni addition on the CuFe-LDO hydrotalcites were investigated by XRD, BET, SEM, H_2-TPR, NH_3-TPD, XPS, and in-situ DRIFTS characterization. Furthermore, the reaction pathways of NH_3 and NO_x adsorption on the surface of the NiCuFe-LDO catalyst and the interaction mechanism between the two reactions were investigated.

Experimental

Catalyst preparation

Co-precipitation method

An accurate quantity of $Ni(NO_3)_2 \cdot 6H_2O$, $Cu(NO_3)_2 \cdot 3H_2O$, and $Fe(NO_3)_3 \cdot 9H_2O$ was weighed and dissolved in 80 mL of deionized water. The molar ratio of $n(Ni^{2+})$: $n(Cu^{2+})$: $n(Fe^{3+})$ was 1:2:1. The solution was ultrasonicated for 50 min and subsequently stirred for 30 min. The pH was adjusted to 9.5 using a solution for pH adjustment. The pH solution was prepared by dissolving 0.6 g of NaOH in 30 mL of distilled water at a concentration of 0.5 mol/L, and 0.159 g of Na_2CO_3 in 30 mL of water at a concentration of 0.5 mol/L. The reaction solution was transferred to a reactor and heated at 110 °C for 12 h. After cooling, the catalyst was washed with deionized water and dried at 80 °C for 12 h to obtain the NiCuFe-LDH precursor. Followed by roasting the precursor in air atmosphere at 400 °C for 2 h to acquire the NiCuFe-LDO catalyst, which was labelled as NiCuFe-LDO-1.

Impregnation method

A suitable amount of $Cu(NO_3)_2 \cdot 3H_2O$ and $Fe(NO_3)_3 \cdot 9H_2O$ were measured and dissolved in 80 mL of deionized water with a molar ratio of $n(Cu^{2+})$: $n(Fe^{3+}) = 2:1$. The mixture was subjected to ultrasonication for 50 min, followed by stirring for 30 min. The pH was adjusted to 6.8 using the pH-adjusting solution mentioned above. The mixture was transferred to a reaction vessel and heated at 110 °C for 12 h. After cooling to room temperature, the product was washed with deionized water, dried, and calcined at 400 °C for 2 h to produce CuFe-LDO. The CuFe-LDO powder was added to 100 ml of deionized water and $Ni(NO_3)_2 \cdot 6H_2O$ was introduced. After undergoing ultrasonication for 50 min, the mixture was stirred at 60 °C for 1 h to ensure the solid was fully dissolved. Following rotary evaporation and drying, the sample was calcined at 400 °C for 2 h. The resulting catalyst was labelled as NiCuFe-LDO-2.

Hydrothermal urea synthesis

An amount of $Ni(NO_3)_2 \cdot 6H_2O$, $Cu(NO_3)_2 \cdot 3H_2O$, $Fe(NO_3)_3 \cdot 9H_2O$ was dissolved in 80 mL of deionized water so that $n(Ni^{2+})$: $n(Cu^{2+})$: $n(Fe^{3+}) = 1:2:1$. Ammonium fluoride was then added to the mixture, followed by the addition of an appropriate amount of urea. The solution underwent 30 min of stirring before being transferred to a reactor and subjected to heating at 110 °C for 12 h. Following cooling to room temperature, the mixture was filtered and washed before being dried in an oven set to 80 °C for 12 h. The dried product was then ground to form a fine powder, resulting in the formation of NiCuFe-LDH. The precursor powder was subsequently

roasted at 400 °C for 2 h, resulting in the formation of the NiCuFe-LDO catalyst, labelled NiCuFe-LDO-3.

Catalyst characterization

X-ray diffraction analysis (XRD) was used to characterising the crystal structure of the samples with a Bruker D8 model X-ray diffractometer. The nitrogen physical adsorption–desorption test was used to characterize the specific surface area and pore structure of the catalysts, which were determined using a Jing micro Gobo JW-BK132F analyzer. The samples were degassed under vacuum at 250 °C for 2.5 h prior to the measurement, and the BET specific surface area and micropore volume of the samples were calculated using the BET method and t-line graph method. Scanning electron microscopy (SEM) was used to investigate the morphological characteristics of the samples by SU8010 Hitachi. X-ray photoelectron spectroscopy (XPS) was carried out using a Thermo Scientific 250Xi multifunctional photoelectron spectrometer to determine the elemental distribution and state on the surface of the catalyst.

Hydrogen Programmed Temperature Rise Reduction (H_2-TPR) characterization tests were carried out using a Peotek PCA-1200 Programmed Temperature Rise Chemisorption Instrument to analyze the redox properties of the catalysts. The sample to be tested was accurately weighed (100 mg) and pretreated under a 5% O_2/N_2 atmosphere at 400 °C for 1 h. Subsequently, H_2 reduction was carried out under a 5% H_2/N_2 atmosphere and a gas flow rate of 30 mL/min. Ammonia programmed temperature rising adsorption and desorption (NH_3-TPD) characterization tests were carried out using a Peard programmed temperature rising chemisorption instrument to characterize the surface acidity of the catalyst. 100 mg of the sample to be tested was accurately weighed and pretreated with helium for 1 h at 400 °C. After pretreatment, NH_3 adsorption was carried out at 100 °C. The adsorption gas: 1% NH_3/He. After adsorption, the sample was purged with helium for 30 min and finally NH_3 desorption was carried out.

In situ infrared spectroscopy (in situ DRIFTS) experiments were conducted on a Bruker TENSOR II spectrometer to analyze NH_3 or ($NO+O_2$) adsorption on various catalysts. Prior to the in-situ DRIFTS characterization, the catalysts underwent pretreatment in an N_2 flow of 100 mL min^{-1} at 400 °C for 30 min, and the spectra were recorded by subtracting the background spectra acquired from treated catalysts with an N_2 flow. NH_3 absorption spectra of the catalysts exposed to a gas mixture of 1100 ppm NH_3 and N_2 (balance) flowing at 100 mL min^{-1} were recorded. ($NO+O_2$) adsorption spectra of the catalysts exposed to a gas mixture of 1000 ppm $NO+4V\%$ O_2+N_2 (balance) flowing at 100 mL min^{-1} were measured.

NH_3-SCR activity evaluation

Catalyst samples were evaluated in a quartz-based fixed bed microreactor tube. A mixture of 300 mg catalyst and 300 mg quartz sand was prepared for the NH_3-SCR reaction in the microreactor. The simulated exhaust gas was comprised of 1100 ppm

NH_3, 1000 ppm NO, 4 V% O_2, 5.0 V% H_2O, and N_2 (balance). The gas volume was 500 mL/min, with an airspeed of 100,000 mL/ (g h). The concentration of NO was measured using a MODEL1080 analyzer. The NO conversion and N_2 selectivity were calculated from the concentration of NO before and after the catalyst bed at a steady state as follows:

$$NO\,conversion\% = \frac{[NO]_{in} - [NO]_{out}}{[NO]_{in}} \times 100\%$$

$$N_2 selectivity(\%) = \frac{[NO]_{in} + [NH_3]_{in} - [NO_2]_{out} - 2[N_2O]_{out}}{[NO]_{in} + [NH_3]_{in}} \times 100\%$$

# Results and discussion

XRD analysis

The XRD patterns in Fig. 1a show that all three precursors for the NiCuFe-LDH samples have similar profiles, and the characteristic reflections of hydrotalcite are clearly detectable. The (003), (006), and (012) crystal planes of the LDHs are evident at 2θ = 12.2°, 23.0°, and 34.5°. Additionally, the diffraction peaks near 2θ = 39°, 47°, 60°, and 62° belong to the (015), (018), (110), and (113) planes [17], which are characteristic peaks of the hydrotalcite-like compounds. This indicates high purity and good crystallinity of the hydrotalcite.

The crystal structure of NiCuFe-LDO samples was investigated by XRD analysis, as shown in Fig. 1b. The CuFe-LDO sample exhibited CuO diffraction peaks at 32.5°, 35.5°, 38.7°, and 48.7°, while Fe_2O_3 diffraction peaks were observed at 62.8° and 75.5°. The NiCuFe-LDO catalysts, synthesized by the three methods, displayed the typical diffraction peaks of hydrotalcite, with the peak intensities appearing to decrease. This signifies that the three synthesis methods did not destroy the original crystalline structure, but the active species on the surface of the sample interacted with the carrier and reduced the carrier order.

NiCuFe-LDO samples exhibited diffraction peaks of NiO at 37.1°, 43.1°, 63.6°, and 79.1°, as well as diffraction peaks attributed to $NiFe_2O_4$ at around 30.2°. This observation suggests successful Ni penetration into the CuFe-LDO interlayer structure. The characteristic diffraction peaks of the NiCuFe-LDO-3 sample was significantly stronger than the other samples, indicating better crystallinity.

SEM analysis

The morphology of the three hydrotalcite samples can be directly shown in Fig. S1 by observation through SEM. The NiCuFe-LDOs produced by the three different synthesis methods all exhibit a "petal-like" hydrotalcite-like morphology [18]. This is attributed to the clustering of hydrotalcite layers, while laminates continue to
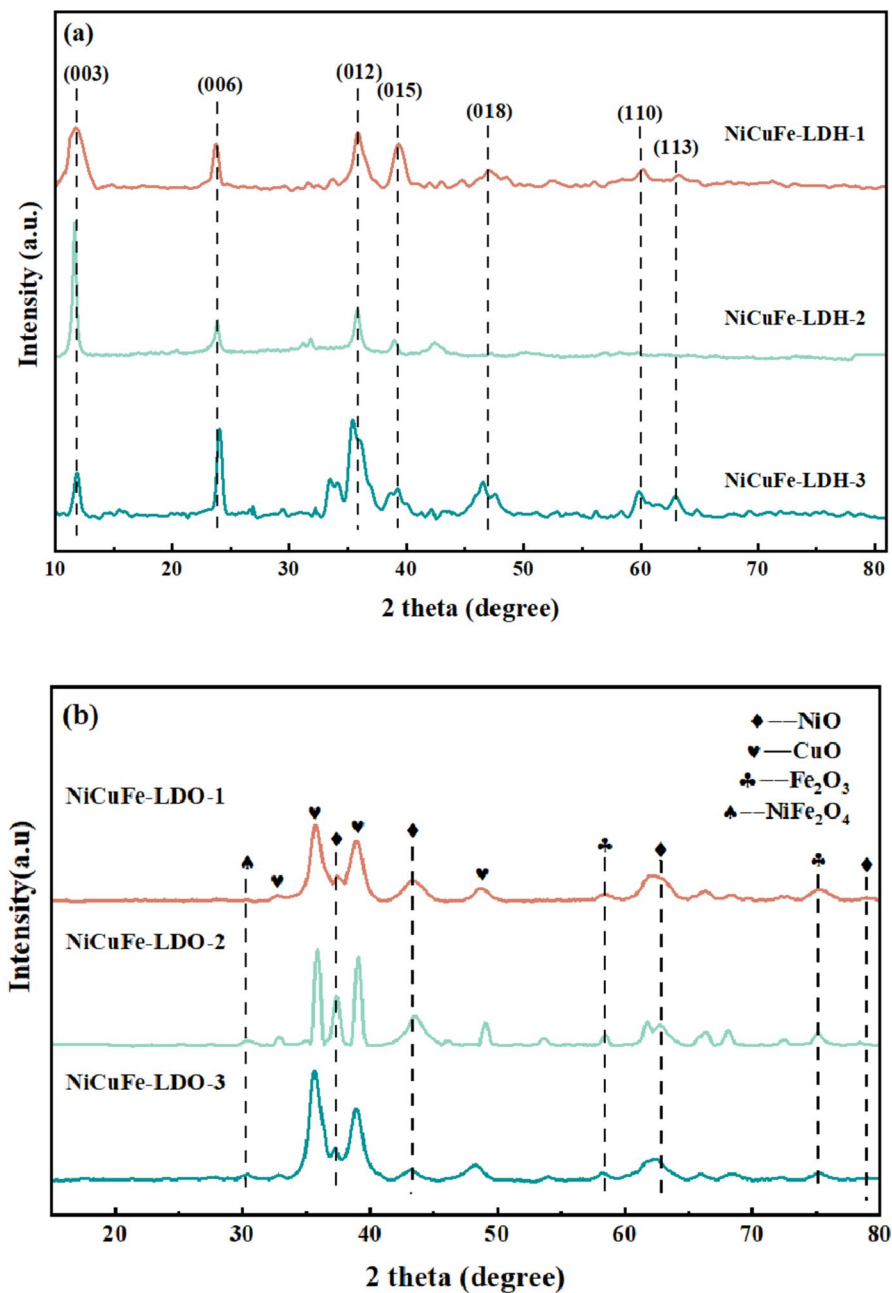
Fig. 1 XRD patterns of LDO samples. **a** XRD spectrogram of the NiCuFe-LDO catalysts without calcination; **b** XRD analysis of the NiCuFe-LDO at 400 °C calcination temperatures

grow on the crystalline surface, which is typical of the hydrotalcite structure. The SEM results are consistent with the XRD results, which means that the NiCuFe-LDO catalyst was synthesized successfully.

Further comparing Fig. S1a-S1b with Fig. S1c, it is evident that the hydrotalcite in Fig. S1a-S1b displays smaller grain sizes and does not undergo significant crystalline surface growth. The poor crystallinity leads to a larger longitudinal scale between the lamellae and the formation of spherical features on the sample surface. The variances in the resulting products could be ascribed to the use of carbonate and nitrate ions become the inhibitors, which hindered the crystalline growth and affected the morphology [19]. Furthermore, the rivalry among OH^-, CO_3^{2-}, and NO_3^- could also impact the morphology and crystallinity of hydrotalcite [20]. The morphology in Fig. S1c demonstrates that the sample that underwent the urea hydrothermal method exhibits a delicate petal-shaped structure. The structure is assembled from irregularly intersecting nanosheets with thinned and slightly curled layers, which effectively mitigates the stacking of laminates, thus resulting in better dispersion of theactivity sites.

The EDS distributions of the catalysts are also shown in Fig. S1, and the atomic distribution of the samples are shown in Fig. S2. As is evident from that the Ni, Cu, and Fe elements are uniformly distributed in the NiCuFe-LDO catalysts produced by the three synthesis methods, indicating that the Ni element is successfully doped into the catalyst lattice. Table 1 shows the atomic percentages of the samples. It can be observed that the ratio of Ni, Cu, and Fe elements in the three samples roughly follows the 1:2:1 ratio.

BET analysis

Alterations in the physical structure and properties of the catalysts have an impact on the NH_3-SCR activity. The CuFe-LDO and NiCuFe-LDO catalysts underwent N_2 adsorption–desorption characterization to analyze the impact of three diverse synthesis methods on catalyst parameters, including the specific surface area and volume of micropores. Fig. S3 illustrates the nitrogen adsorption–desorption isotherms for the catalysts. The isotherms of all samples exhibited standard type I adsorption–desorption isotherms. The test points were sharply inclined at low relative pressures ($P/P_0 < 0.02$) and then flattened out, indicating that the catalysts are porous materials with mesopores, highly concentrated microporous distributions, and regular pore structures. In addition, it was found that the hysteresis loops of all catalysts were consistent with H_3-type hysteresis loops, which were observed at higher

Table 1 Atomic percentage of NiCuFe-LDO samples	NiCuFe-LDO-1	NiCuFe-LDO-2	NiCuFe-LDO-3
Ni	24.99	27.94	27.49
Cu	48.32	45.31	46.70
Fe	26.69	26.75	25.81
Total	100.00	100.00	100.00

relative pressure ranges. This suggests that the interlayer structure is well-preserved and exhibits a typical cleavage shape. The N_2 adsorption–desorption isotherms of the NiCuFe-LDO catalyst samples, which were synthesized by three different methods, were comparable to those of the CuFe-LDO sample. This indicates that the synthesis methods did not significantly impact the pore structure of the original sample, which still maintained the slit-like microporous structure.

Table 2 shows the structural properties of NiCuFe-LDO catalysts produced via various synthesis methods. NiCuFe-LDO-1 and NiCuFe-LDO-3 exhibited a significant advantage over the original sample in terms of specific surface area, microporous volume, and pore size. Conversely, the specific surface area of NiCuFe-LDO-2 decreased as compared to the initial sample, which amounted to 74 m²/g. The incorporation of nickel in the synthesis of CuFe-LDO by impregnation disrupts the pore structure of the catalyst. The analysis indicates a strong correlation between the catalytic activity and the specific surface area and microporous volume. Optimization of the reactant conversion can be achieved when both factors are maximized.

XPS analysis

X-ray photoelectron spectroscopy is a versatile method of surface analysis that is commonly used to assess the chemical state of catalyst surfaces. The XPS spectra of Ni 2p, Cu 2p, Fe 2p, and O 1s were obtained by fitting their energy spectra with peak splitting. The surface contents were then calculated from their peak areas.

According to the literature [21, 22], Fig. S4b shows that the peaks between 933.1 and 933.5 eV correspond to CuO, while the peaks between 936.1 and 936.6 eV represent isolated Cu^{2+} ions. Among copper species on the surface of the NiCuFe-LDO-3 catalyst, Cu^{2+} was present in the highest distribution (37.48%). Cu^{2+} played a crucial role in improving the low-temperature denitrification performance of the catalyst. This resulted in the catalyst having the best catalytic activity among those prepared by the urea hydrothermal method, as verified in subsequent activity tests [23].

The Ni 2p3/2 spectra of all catalysts were analyzed in Fig. S4a and S4c, with peak splitting to identify three distinct peaks located at 854.6, 856.0–856.2, and 860.4–861.3 eV. The identified peaks were representative of Ni^{2+} and Ni^{3+} as well as satellite peaks [10]. The Fe 2p3/2 peak splits into two peaks at 710.9 and 713.8 eV, with assignments to the FeO and Fe_2O_3 species [24]. Iron species were mainly present on the catalyst surface in the form of Fe^{3+} and a small proportion of Fe^{2+}.

Table 2 BET surface areas and pore volumes of the samples	Samples	Surface area (m²/g)	Micropore volum (cm³/g)	Pore size (nm)
	CuFe-LDO	110	0.185	6.720
	NiCuFe-LDO-1	123	0.282	8.438
	NiCuFe-LDO-2	74	0.144	7.762
	NiCuFe-LDO-3	129	0.341	10.506

**Table 3** Elemental states and species proportions on the surface of the samples

Samples	$Ni^{2+}/(Ni^{3+}+Ni^{2+})$	$Cu^{2+}/(Cu^{2+}+CuO)$	$Fe^{3+}/(Fe^{3+}+Fe^{2+})$	$O_\beta/(O_\beta+O_\alpha)$
NiCuFe-LDO-1	60.15	34.43	65.48	33.45
NiCuFe-LDO-2	65.95	26.40	49.14	26.84
NiCuFe-LDO-3	68.96	37.48	75.16	44.52

As indicated in Table 3, the NiCuFe-LDO-3 catalyst displayed a higher Fe^{3+} content on its surface compared to the other catalysts, with Fe^{3+} making up 75.16% of the surface content. Furthermore, the NiCuFe-LDO-3 catalyst exhibited the highest concentration of Ni^{2+} and the lowest concentration of Ni^{3+}. Conversely, the Fe^{2+} to Fe^{3+} ratio on the surface of the impregnated NiCuFe-LDO-2 sample was approximately 1:1, with a higher presence of Fe^{2+} species compared to the samples synthesized by the other two methods. The synthesis made by the urea hydrothermal and co-precipitation methods was thought to promote the redox reaction of Ni and Fe ions in $NiFe_2O_4$ spinel ($Ni^{3+}+Fe^{2+} \leftrightarrow Ni^{2+}+Fe^{3+}$), thus leading to the conversion of more Fe^{2+} to Fe^{3+}. Additionally, the interactions in the bimetallic oxides were believed to enhance the formation of a redox cycle, which further improves the denitrification activity of the catalysts [14, 25]. When Ni was impregnated on the surface of the CuFe-LDO sample by the impregnation method, the redox reaction between Ni and Fe ions did not occur or occurred at a low level, resulting in the poor NH_3-SCR activity of the sample, which was even slightly lower than that of the original sample.

Two spectral peaks situated between 530.2–530.6 eV and 531.5–531.9 eV could be identified by split-peak fitting for O1s. These peaks were attributed to lattice oxygen (O_α) and chemisorbed oxygen (O_β). Based on previous research [26], chemisorbed oxygen was the most efficient oxygen species in the NH_3-SCR reaction. The oxygen species presented in the gas-phase oxygen molecules that adsorbed on the catalyst surface were more liable to be exchanged and migrated with chemisorbed oxygen O_β. This beneficially affected the NH_3-SCR reaction [27]. The findings from Fig. S4d and Table 3 indicated that NiCuFe-LDO-3 sample exhibited a greater percentage of chemisorbed oxygen species O_β on their surface compared to NiCuFe-LDO-1 and NiCuFe-LDO-2 samples. The increased availability of chemisorbed oxygen facilitates the oxidation of NO to NO_2, thus facilitating the "Fast-SCR" reaction ($2NH_3+NO+NO_2 \rightarrow 2N_2+3H_2O$) and ultimately enhancing SCR performance. Correspondingly, this represented one of the crucial contributing factors to the superior NH_3-SCR activity of the NiCuFe-LDO-3 sample.

H_2-TPR analysis

The reduction performance of the catalysts was assessed using the H_2-TPR method and the results of the characterization were shown in Fig. 2. Five reduction peaks of all the NiCuFe-LDO catalysts appeared at approximately 250 °C, 340 °C, 440 °C, 500 °C and 600 °C. The reduction process of CuO is attributed to the strong
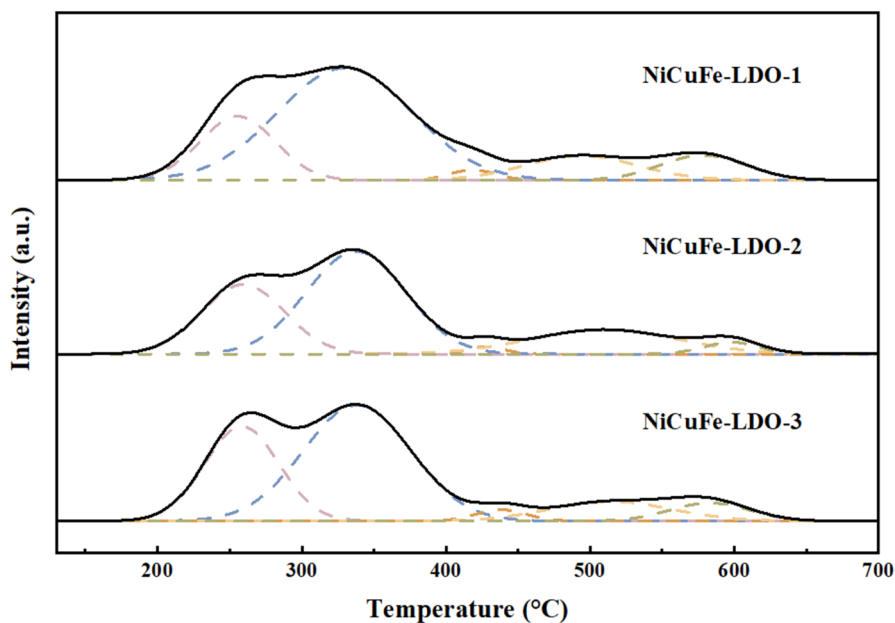
Fig. 2 H_2-TPR profiles of the NiCuFe-LDO samples

reduction peak around 250 °C [28], and the reduction peaks relate to the reduction of a highly dispersed copper oxide material, which can be specifically classified as $Cu^{2+} \rightarrow Cu^{+}$ and $Cu^{+} \rightarrow Cu^{0}$ [29, 30].

The peaks observed at temperatures approximately 340 °C can be attributed to the reduction of $Ni^{2+}/(Ni^{3+})$ to Ni^{0}. Additionally, the reduction peaks at around 440 °C can be related to the synergistic reduction of $Fe^{3+} \rightarrow Fe^{2+}$ as well as various Ni and Fe components [31]. The literature indicates that the peaks appearing at approximately 500 °C are due to the reduction of the $NiFe_2O_4$ phase and the reduction of relatively free NiO material [32]. Finally, the peaks at around 600 °C are attributed to the reduction process of $Fe^{2+} \rightarrow Fe$ [33].

Following quantitative analysis, the H_2 consumption for each sample during the reduction reaction was obtained. The results were presented in Table 4, with the highest H_2 consumption observed in the NiCuFe-LDO-3 sample (4.576 mmol/g),

Table 4 H_2-TPR quantitative analysis

	Reduction peak temperature (°C)					Hydrogen consumption(mmol/g)
	Peak 1	Peak 2	Peak 3	Peak 4	Peak5	
NiCuFe-LDO-1	259	336	420	499	579	3.388
NiCuFe-LDO-2	260	338	428	506	600	3.264
NiCuFe-LDO-3	258	338	438	514	582	4.576

followed by NiCuFe-LDO-1 (3.388 mmol/g) and NiCuFe-LDO-2 (3.264 mmol/g). Prior research asserted that a higher hydrogen consumption of the catalyst equates to superior redox performance and more active materials [34]. Thus, it could be inferred that NiCuFe-LDO-3 exhibits favorable synergistic effects, which enhance the redox potential. This might account for its superior catalytic activity compared to other samples.

NH$_3$-TPD analysis

To examine the impact of diverse synthesis methods on the surface acidity of the catalysts, the NH$_3$-TPD characterization technique was employed. Figure 3 presented the obtained outcomes. All the samples exhibited three desorption peaks, namely a low-temperature peak at 200 °C, a medium-temperature peak at 300 °C, and a high-temperature peak at approximately 500 °C. The literature suggests that the desorption peak at 200 °C indicates weak NH$_3$ adsorption, which occurs via NH$_3$ adsorbed on the surface hydroxyl group of the weak Lewis acidic site [35]. The desorption peak at 350 °C represented a strong Lewis acidic site of NH$_3$ adsorption, which was formed through Cu ion exchange [13]. The high-temperature desorption peak at or above 500 °C was indicative of Brønsted acidic site, which belonged to the medium-strong acidic site [36]. The initial desorption peaks of the samples prepared using the three different synthesis methods were similarly located in the low-temperature
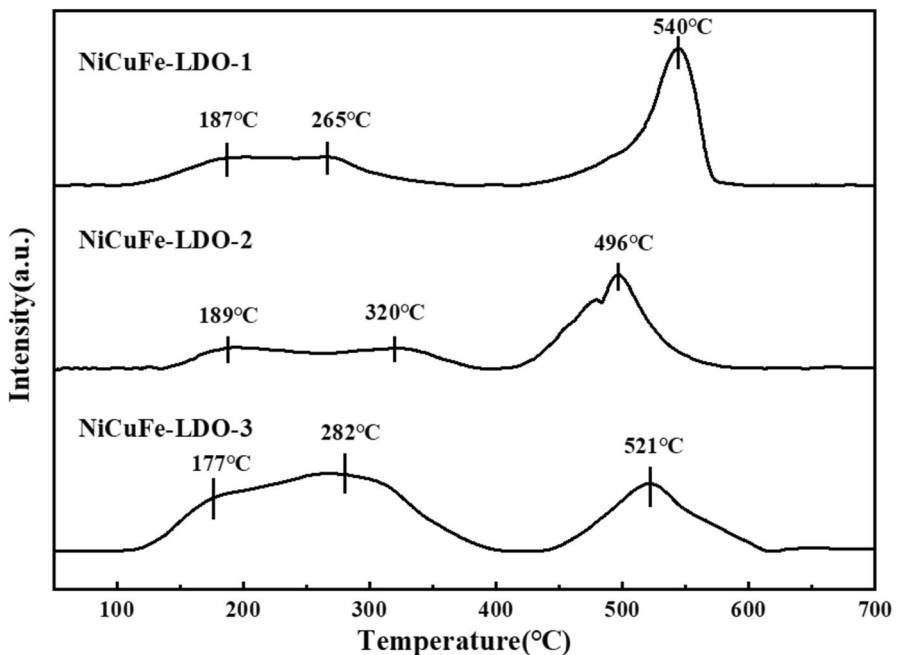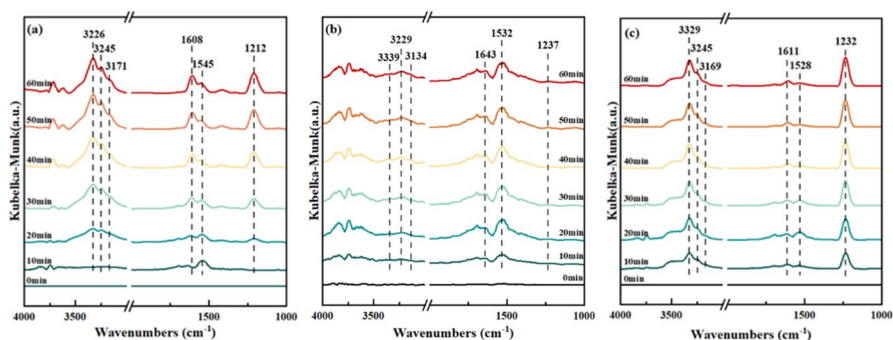

Fig. 3 NH$_3$-TPD profiles of NiCuFe-LDO samples

Table 5 Acidity of the samples calculated from the NH$_3$-TPD profile

Samples	Acidic site ratio (%)		Total acid (%)
	weak acid (< 400 °C)	Strong acid (> 400 °C)	
NiCuFe-LDO-1	45.02	54.98	0.73
NiCuFe-LDO-2	38.86	61.14	0.67
NiCuFe-LDO-3	71.55	28.45	1.00

Fig. 4 In-situ DRIFTS of NH$_3$ adsorption on the NiCuFe-LDO samples at 150 °C. **a** NiCuFe-LDO-1; **b** NiCuFe-LDO-2; **c** NiCuFe-LDO-3. (Conditions:1000 ppm NH$_3$ adsorption)

region, with the NiCuFe-LDO-3 sample having a significantly higher content of weak acids than the NiCuFe-LDO-1 and NiCuFe-LDO-2 samples. This indicates that the active components of the samples from the hydrothermal synthesis of urea are highly dispersed. This promotes complete exposure of the acidic sites, which yields a high NH$_3$ adsorption capacity.

Table 5 presents the total NH$_3$ adsorption capacity and the percentage of each acidic site type based on the integrated peak area. The NiCuFe-LDO-3 catalyst synthesized using the urea hydrothermal method showed the highest total acidic capacity, which increased its potential for NH$_3$ adsorption and activation [37]. In addition, the higher the proportion of catalyst at Lewis acid sites, the more active the catalyst samples are, which is consistent with the denitrification test results.

In-situ DRIFTS analysis

NH$_3$ adsorption analysis results

NH$_3$ adsorption capacity is a fundamental measure of the catalyst surface acidity and plays a vital role in the NH$_3$-SCR reaction. To further determine the type and strength of acidity, in-situ DRIFTS experiments were performed on the samples.

Before NH$_3$ adsorption, the samples were pretreated at high temperatures in a nitrogen atmosphere to eliminate some adsorbed species. The temperature was then

reduced to 15 °C in preparation for the NH_3 adsorption test. The low band range showed three peaks located at 1212–1237, 1528–1545, and 1608–1643 cm^{-1}, which gradually increased with time and then remained constant, as shown in Fig. 4. The asymmetric vibration of NH_4^+ at the Brønsted acidic site was associated with the energy band at 1542 cm^{-1} [38]. Moreover, the peaks at 1210 cm^{-1} and 1612 cm^{-1} were a result of the bending vibration of the N–H bond of the NH_3 ligand at the Lewis acidic site [39]. The peak around 1210 cm^{-1} was ascribed to the NH_3 species adsorbed on the Fe site, while the 1612 cm^{-1} peak was attributed to the NH_3 species adsorbed on the Cu site [40]. The N–H stretching vibrational region at high wave numbers (3100–3400 cm^{-1}) displayed peaks at 3156 cm^{-1} and 3329 cm^{-1} which was attributed to NH_3 adsorbed on Cu active sites [41]. The NH_4^+ adsorption peak was assigned to the peak observed at 3249 cm^{-1} [42]. Adsorption peaks were observed between 3625 and 3636 cm^{-1}, possibly because of a strong interaction between NH_3 and surface hydroxyl groups [43].

The result demonstrates the co-existence of Lewis and Brønsted acidic sites on the surface of NiCuFe-LDO samples. The comparison of the intensity of the two acidic sites indicated that the surface acidic sites in NiCuFe-LDO-1 and NiCuFe-LDO-3 samples mostly consist of Lewis acidic sites. The peak observed at 1532 cm^{-1} in NiCuFe-LDO-2 was higher than that seen in the other two samples. Additionally, the peak at 1237 cm^{-1} was significantly lower, suggesting that the surface acidic sites of this specific sample consisted mainly of Brønsted acidic sites. This finding is in line with the NH_3-TPD characterisation results. The NH_3-SCR reaction is promoted by the stronger adsorption of activated NH_3 on the Lewis acidic site, which is the primary active site. This explains the high activity levels found in the NiCuFe-LDO-1 and NiCuFe-LDO-3 samples.

$NO + O_2$ adsorption analysis results

In-situ DRIFTS desorption experiments were conducted to examine the adsorption and desorption behaviour of NO_x species on the surface of the NiCuFe-LDO-1 catalyst. Upon introducing $NO + O_2$, absorption peaks at 1651, 1563, 1534, 1437, 1380,
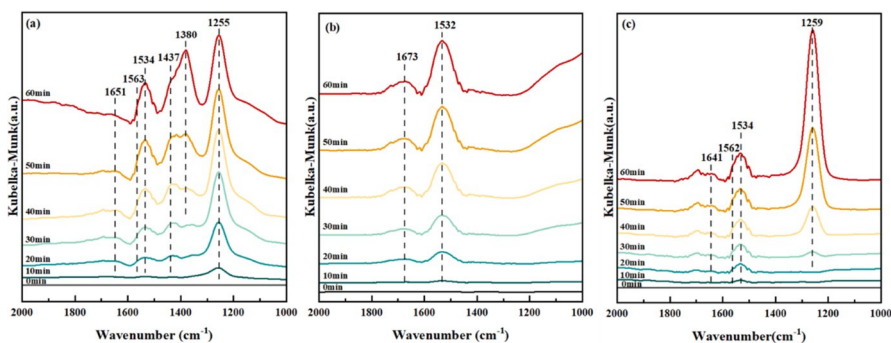
Fig. 5 In-situ DRIFTS of NO_x adsorption on the NiCuFe-LDO samples at 150 °C. **a** NiCuFe-LDO-1; **b** NiCuFe-LDO-2; **c** NiCuFe-LDO-3. (Conditions: 1100 ppm $NO + 4\%$ O_2 adsorption)

and 1255 cm^{-1} were observed on the catalyst surface, as depicted in Fig. 5a. Based on the literature [44–47], the 1617 cm^{-1} peak can be associated with gas-phase or weakly adsorbed NO. The 1534 cm^{-1} peak corresponds to monodentate nitrate while the 1563 cm^{-1} peak belongs to bidentate ligand-type nitrate, resulting from the further oxidation of monodentate nitrate. Finally, the 1255 cm^{-1} peak corresponds to bridge nitrate. A weak infrared absorption peak was observed at 1437 cm^{-1}, indicating that a small amount of nitrite was also formed on the surface of the catalysts obtained through the co-precipitation method. A new adsorption peak at 1355 cm^{-1} appeared after approximately 30 min following the introduction of NO, which was most likely due to ionic nitrate.

The NO + O$_2$ absorption spectra of the NiCuFe-LDO-2 catalyst were quite different from those of the NiCuFe-LDO-1 catalyst, as shown in Fig. 5b. Only one absorption peak of gaseous NO$_2$ molecules could be observed at 1673 cm^{-1} in the sample, and there was no trace of bidentate nitrate. On the other hand, a monodentate nitrate absorption on the peak was detected at 1532 cm^{-1}. The adsorption spectra of NO + O$_2$ on the surface of the NiCuFe-LDO-3 catalyst (Fig. 5c) exhibited similarity with the NiCuFe-LDO-1 catalyst, displaying absorption peaks at 1641, 1562, 1534, and 1259 cm^{-1}. In accordance with the literature [48], these peaks were identified as gaseous NO$_2$ molecules, as bi-dentate, mono-dentate, and bridged nitrate.

When comparing the NO$_x$ adsorption species present of NiCuFe-LDO catalysts, it was observed that bridged nitrate and monodentate nitrate were the prevalent NO$_x$ adsorption species on the surface of NiCuFe-LDO-1 and NiCuFe-LDO-3 catalysts. In contrast, the primary adsorption species present in NiCuFe-LDO-2 catalysts was only monodentate nitrate. Further comparison of NiCuFe-LDO-1 and NiCuFe-LDO-3 catalysts showed that the NiCuFe-LDO-1 sample also showed nitro compounds and ionic nitrates after the passage of NO + O$_2$, which were thermally unstable NO$_x$-derived adsorbent species and were not favourable for NH$_3$-SCR reactions. The literature shows that higher activity levels of nitrites and bridging nitrates in single teeth compared to double teeth [43]. Consequently, the NiCuFe-LDO-3 catalyst produced via urea hydrothermal methodology demonstrated an enhanced NO adsorption capacity, consistent with the results of the NH$_3$-SCR activity assessment.

Pre-absorption of NO + O$_2$ with NH$_3$

To investigate the reaction performance of NiCuFe-LDO catalysts for surface adsorption of nitrogen oxides, in-situ transient reaction experiments at 150 °C were used. The absorption spectra of NiCuFe-LDO-3 catalysts were observed in Fig. S5. The peaks located at 1618, 1589, 1551, and 1255 cm^{-1} were identified as corresponding to the gaseous NO$_2$ molecule, bi-dentate nitrate, uni-dentate nitrate, and bridged nitrate. As the gas changes to NH$_3$, the peak at 1551 cm^{-1} reduces gradually until it disappears, while the peaks of the adsorbed state NH$_3$ species (1631, 1589, 1534 cm^{-1}) increase in intensity [49]. Moreover, it is suggested that the adsorbed nitrate does not readily participate in the reaction, as the peaks at 1631 and 1255 cm^{-1} remain present [50]. As the reaction time increases, the intensity of the absorption peaks also rises, which is attributed to the superposition of NH$_3$ adsorption on the Lewis acidic site [51].

The phenomenon could be attributed to the fact that monodentate nitrate reacts with NH_3 directly, whereas bidentate nitrate was not significantly involved in the NH_3-SCR reaction. Therefore, monodentate nitrate formed on the surface of the NiCuFe-LDO samples could be considered as the primary reactive intermediate species that could react directly with NH_3 to produce N_2 and H_2O. It is evident that adsorbed NO_x species can participate in the denitrification reaction via the L–H pathway with NH_3 [52].

Pre-adsorption of NH_3 with $NO + O_2$

The in-situ DRIFTS results for the adsorption of NH_3 on NiCuFe-LDO catalysts at 150 °C, followed by the reaction with $NO + O_2$ are presented in Fig. S6. As illustrated in the figure, NiCuFe-LDO catalyst, exposed to NH_3 following adsorption saturation and N_2 flushing, exhibited the peaks of NH_3 species at 1631, 1535, and 1229 cm^{-1} [53, 54]. When $NO + O_2$ was passed through, the absorption peaks of the adsorbed NH_3 species at 1229 cm^{-1} and 1631 cm^{-1} reduced swiftly and vanished after 5 min, along with the absorption peak at 1535 cm^{-1}. The observation suggests that NO_x species reacted primarily with the adsorbed state NH_3 on the Lewis acidic site, followed by the reaction of NH_3 adsorbed on the Brønsted acidic site. The disappearance of both NH_3 adsorbed species indicates that both types of ammonia species adsorbed on the acidic site can engage in both the NH_3-SCR reaction and the NO reduction, as part of the E-R reaction mechanism [55]. The NH_4^+ absorption peak attributed to Brønsted acidic sites at 1440 cm^{-1} slightly increased following the passage of $NO + O_2$ for 5 min. This outcome was due to the transformation from the adsorbed state of NH_3 on Lewis acidic sites to NH_4^+ adsorbed state of NH_3 to NH_4^+ under the effect of $NO + O_2$. Thus, the outcome implies that the NiCuFe-LDO catalyst possesses a well NH_3 adsorption and activation ability. As a result, it enhances the reaction rate between NH_3 species and $NO + O_2$, thereby facilitating the NH_3-SCR reaction.

The results of the transient reaction experiments conducted in-situ indicate that NO gas molecules can react directly with $-NH_2$ (E-R mechanism) and can also be converted into nitro species via oxygen adsorbed on the catalyst surface, followed by reaction with $–NH_2$ (L–H mechanism) [56]. This clarifies that the NiCuFe-LDO catalysts induce the low-temperature NH_3-SCR denitrification process through the combined influences of the E–R and L–H pathways.

Mechanism study

The NH_3-SCR reaction over the NiCuFe-LDO catalyst synthesized by urea hydrothermal method was found to follow both the E–R and L–H mechanisms as analyzed in the previous section. The NiCuFe-LDO-3 catalyst has a higher number of Lewis acidic sites. NH_4^+ and its dehydrogenation intermediate ($–NH_2$) are more active than NH_3 in the coordination state. This allows them to preferentially react with NO to produce NH_2NO. The reaction of NH_4^+/NH_3 with NO produces NH_3HNO/NH_3NO, which further decomposes to NH_2NO. Ultimately, N_2 and H_2O are decomposed,

consistent with the E-R mechanism [54]. When adsorbed NH_3 reacts with nitrate, NO can be adsorbed and bound to the surface of metal oxides to form monodentate nitrate species. These species further react with the ligand-adsorbed NH_3 to form N_2 and H_2O. The NiCuFe-LDO-3 sample has the largest number of monodentate nitrate species, which is conducive to the "fast SCR" reaction. The L–H mechanism is followed [55].

Evaluation of the activity of catalyst NH_3-SCR reaction

Figure 6a presents a comparison of the catalytic activity of various NiCuFe-LDO catalysts that underwent different synthesis methods. The results show that the NiCuFe-LDO-2 sample synthesized by the impregnation method exhibited the lowest catalytic activity. The highest NO conversion rate of the NiCuFe-LDO-2 sample was seen at 240 °C and reaching 82% only, which was lower than that of the original CuFe-LDO catalyst without Ni at the 160 °C to 300 °C temperature range. The reduced activity may be due to changes made to the initial CuFe-LDO sample, which disrupted its ion distribution on the surface or blocked the active site. The NiCuFe-LDO-1 sample obtained through the co-precipitation technique exhibited only minor improvement in $deNO_x$ activity at lower temperatures compared to the CuFe-LDO catalyst. The NiCuFe-LDO-3 sample, synthesized by the urea hydrothermal route exhibited the greatest catalytic activity. It achieved a NO conversion rate of more than 80% within the temperature range of 180 °C to 280 °C, and the NO conversion at 240 °C was up to 95%. Although the catalytic activity of the sample decreases slightly with temperature, a conversion of 74% is maintained at 300 °C, demonstrating a greatly extended temperature window. In summary, the introduction of Ni was found to effectively enhance the activity of the CuFe-LDO catalyst and broaden the temperature range for improved high-temperature catalytic activity. Notably, the activity of samples with Ni introduced through different methods exhibits significant variations, and the urea hydrothermal route was the best.
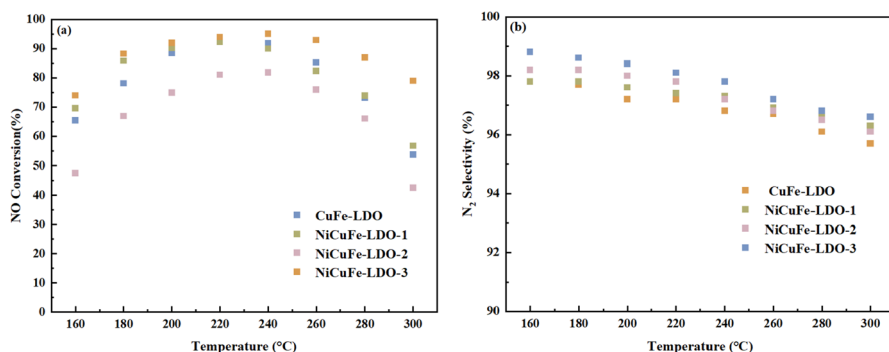
Fig. 6 NH_3-SCR performance of LDO samples. **a** Nitrogen oxide (NO_x) conversion; **b** N_2 selectivity. (Reaction conditions: NO = 1000 ppm, NH_3 = 1100 ppm, O_2 = 4%, H_2O = 5%, balanced N_2, and GHSV = 100,000 h.$^{-1}$)

Figure 6b demonstrates that all samples exhibit over 95% N_2 selectivity at 150~300 °C. The NiCuFe-LDO-3 sample shows slightly better selectivity than the other samples. In addition, in order to evaluate the effect of 5% water in the simulated gas on the catalyst, the reacted catalyst, named NiCuFe-LDO-3a, was removed and subjected to XRD tests. The results are presented in Fig. S7. The absence of characteristic LDH peaks in NiCuFe-LDO-3a suggests that the hydrotalcite has not been reduced. The catalysts appear to be minimally affected by the presence of a small amount of water, which can be disregarded.

Conclusion

The study describes the production of NiCuFe-LDO catalysts using co-precipitation, impregnation, and urea hydrothermal methods. Structural analysis shows that the NiCuFe-LDO-3 sample has a significant specific surface area and a highly crystalline nanoflower-shaped structure, which provides more reactant adsorption sites and enhances NH_3-SCR activity. The NiCuFe-LDO-3 catalyst exhibited the highest concentration of Lewis acidic sites, as indicated by the H_2-TPR and NH_3-TPD analyses, resulting in the most substantial hydrogen consumption. The presence of Lewis acid was found to be crucial in the NH_3-SCR reaction, which was supported by in-situ DRIFTS characterization. Additionally, XPS characterization revealed ionic transformations on the surface of samples. The sample created using the urea hydrothermal technique contained higher amounts of Ni^{2+}, Fe^{3+}, and chemisorbed oxygen, resulting in a higher conversion rate and a broader temperature range. Additionally, the reaction mechanism of the NiCuFe-LDO catalyst was revealed through in-situ infrared spectroscopy, which showed the combined action of the E-R pathway and the L–H pathway. The results indicate that the NiCuFe-LDO-3 samples synthesized by the urea hydrothermal method exhibit the best catalytic properties and have significant potential for practical use.

References

1. Wang H, Yuan B, Hao R, Zhao Y, Wang X (2019) A critical review on the method of simultaneous removal of multi-air-pollutant in flue gas. Chem Eng J. https://doi.org/10.1016/j.cej.2019.122155
2. Wang D, Chen Q, Zhang X, Gao C, Wang B, Huang X, Peng Y, Li J, Lu C, Crittenden J (2021) Multipollutant control (MPC) of flue gas from stationary sources using SCR technology: a critical review. Environ Sci Technol 55(5):2743–2766. https://doi.org/10.1021/acs.est.0c07326

3.   Wang J, Zhu C, Li B, Gong Z, Meng Z, Xu G, Wu W (2020) Prepare a catalyst consist of rare earth minerals to denitrate via NH_3-SCR. Green Process Synth 9(1):191–202. https://doi.org/10.1515/gps-2020-0020

4.   Xu J, Zou X, Chen G, Zhang Y, Zhang Q, Guo F (2021) Tailored activity of Ce-Ni bimetallic modified V_2O_5/TiO_2 catalyst for NH_3-SCR with promising wide temperature window. Vacuum. https://doi.org/10.1016/j.vacuum.2021.110384

5.   Yuan B, Mao X, Wang Z, Hao R, Zhao Y (2020) Radical-induced oxidation removal of multi-air-pollutant: A critical review. J Hazard Mater. https://doi.org/10.1016/j.jhazmat.2019.121162

6.   Zhang Y, Xiong Z, Yang Q, Zhou F, Lu W, Shi H (2022) Influence of copper doping on the low-medium NH_3-SCR activity of magnetic W/Fe_2O_3 catalyst: its synergetic effect of glucose dosage. J Environ Chem Eng. https://doi.org/10.1016/j.jece.2022.108694

7.   Wang P, Sun H, Quan X, Chen S (2016) Enhanced catalytic activity over MIL-100(Fe) loaded ceria catalysts for the selective catalytic reduction of NO_x with NH_3 at low temperature. J Hazard Mater 301:512–521. https://doi.org/10.1016/j.jhazmat.2015.09.024

8.   Zhao L, Huang Y, Zhang J, Jiang L, Wang Y (2020) Al_2O_3-modified CuO-CeO_2 catalyst for simultaneous removal of NO and toluene at wide temperature range. Chem Eng J. https://doi.org/10.1016/j.cej.2020.125419

9.   Xiong P, Zhang H, Li G, Liao C, Jiang G (2021) Adsorption removal of ibuprofen and naproxen from aqueous solution with Cu-doped Mil-101(Fe). Sci Total Environ. https://doi.org/10.1016/j.scitotenv.2021.149179

10. Wan Y, Zhao W, Tang Y, Li L, Wang H, Cui Y, Gu J, Li Y, Shi J (2014) Ni-Mn bi-metal oxide catalysts for the low temperature SCR removal of NO with NH_3. Appl Catal B 148:114–122. https://doi.org/10.1016/j.apcatb.2013.10.049

11. Yan J, Zhao L, Huang Y, Zhang J, Tang J (2022) Mechanistic effect of SO_2 on mesoporous $CuFeAlZrO_x$ catalyst for simultaneous removal of Hg^0 and NO at wide temperature range. Fuel. https://doi.org/10.1016/j.fuel.2022.125424

12. Jiang J, Pan H, Sun G, Ye Q, Shao Z, Shi Y (2011) Promotion of Ni/H-BEA by Fe for NO_x reduction with propane in a lean-burn condition. Energy Fuels 25(10):4377–4383. https://doi.org/10.1021/ef200770f

13. Zhao K, Meng J, Lu J, He Y, Huang H, Tang Z, Zhen X (2018) Sol-gel one-pot synthesis of efficient and environmentally friendly iron-based catalysts for NH_3-SCR. Appl Surf Sci 445:454–461. https://doi.org/10.1016/j.apsusc.2018.03.160

14. Wang R, Wu X, Zou C, Li X, Du Y (2018) NO_x Removal by selective catalytic reduction with ammonia over a hydrotalcite-derived NiFe mixed oxide. Catalysts. https://doi.org/10.3390/catal8090384

15. Wu X, Ci C, Du Y, Liu X, Li X, Xie X (2018) Facile synthesis of NiAl-LDHs with tunable establishment of acid-base activity sites. Mater Chem Phys 211:72–78. https://doi.org/10.1016/j.matchemphys.2018.02.015

16. Li X, Du Y, Guo X, Wang R, Hou B, Wu X (2019) Synthesis of a novel NiMnTi mixed metal oxides from LDH Precursor and its catalytic application for selective catalytic reduction of NO_x with NH_3. Catal Lett 149(2):456–464. https://doi.org/10.1007/s10562-018-2626-7

17. Chen W, Wu B, Wang Y, Zhou W, Li Y, Liu T, Wang S (2021) Deciphering the alternating synergy between interlayer Pt single-atom and NiFe layered double hydroxide for overall water splitting. Energ Environ Sci 14(12):6428–6440. https://doi.org/10.1039/d1ee01395e

18. Song Z, Meng Q, Wei F, Yin Q, Sui Y, Qi J (2023) In situ hydrolysis strategy to synthesis ultrathin CoNi- LDH nanoflowers for High-performance supercapacitors. J Electroanal Chem. https://doi.org/10.1016/j.jelechem.2023.117379

19. Xu R, Zeng HC (2003) Dimensional control of cobalt-hydroxide-carbonate nanorods and their thermal conversion to one-dimensional arrays of Co_3O_4 nanoparticles. J Phys Chem B 107(46):12643–12649. https://doi.org/10.1021/jp035751c

20. Sun X, Wang G, Sun H, Lu F, Yu M, Lian J (2013) Morphology controlled high performance supercapacitor behaviour of the Ni-Co binary hydroxide system. J Power Sour 238:150–156. https://doi.org/10.1016/j.jpowsour.2013.03.069

21. Zhang R, McEwen J, Kollar M, Gao F, Wang Y, Szanyi J, Peden C (2014) NO Chemisorption on Cu/SSZ-13: A Comparative Study from Infrared Spectroscopy and DFT Calculations. ACS Catal 4(11):4093–4105. https://doi.org/10.1021/cs500563s

22. Xue H, Guo X, Wang S, Sun C, Yu J, Mao D (2018) Poisoning effect of CaO on Cu/ZSM-5 for the selective catalytic reduction of NO with NH_3. Catal Commun 112:53–57. https://doi.org/10.1016/j.catcom.2018.04.020

23. Gorecka S, Pacultova K, Gorecki K, Smykalova A, Pamin K, Obalova L (2020) Cu-Mg-Fe–O–(Ce) complex oxides as catalysts of selective catalytic oxidation of ammonia to dinitrogen (NH_3-SCO). Catalysts. https://doi.org/10.3390/catal10020153

24. Nedyalkova R, Kamasamudram K, Currier N, Li J, Yezerets A, Olsson L (2013) Experimental evidence of the mechanism behind NH_3 overconsumption during SCR over Fe-zeolites. J Catal 299:101–108. https://doi.org/10.1016/j.jcat.2012.11.009

25. Chin S, Park E, Kim M, Jeong J, Bae G, Jurng J (2011) Preparation of TiO_2 ultrafine nanopowder with large surface area and its photocatalytic activity for gaseous nitrogen oxides. Powder Technol 206(3):306–311. https://doi.org/10.1016/j.powtec.2010.09.035

26. Yang Y, Zhang D, Ji W, Bi F, Song L, Zhang X (2022) Uniform platinum nanoparticles loaded on Universiteteti Oslo-66 (UiO-66): Active and stable catalysts for gas toluene combustion. J Colloid Interface Sci 606:1811–1822. https://doi.org/10.1016/j.jcis.2021.08.127

27. Fang Z, Gao L, Chen H, Liang K, Liu Z, Guan Z, Zhang J (2020) XPS study of probing evidence for displacive disorder in Ni-doped bismuth magnesium niobate pyrochlore. Mater Sci Eng B-Adv. https://doi.org/10.1016/j.mseb.2020.114601

28. Wang Z, Wang L, He F, Jiang Z, Xiao T, Zhang Z (2014) Catalytic soot oxidation over Ce- and Cu-doped hydrotalcites-derived mesoporous mixed oxides. J Nanosci Nanotechnol 14(9):7087–7096. https://doi.org/10.1166/jnn.2014.8944

29. Chen B, Xu R, Zhang R, Liu N (2014) Economical way to synthesize SSZ-13 with abundant Ion-exchanged Cu^+ for an extraordinary performance in selective catalytic reduction (SCR) of NO_x by ammonia. Environ Sci Technol 48(23):13909–13916. https://doi.org/10.1021/es503707c

30. Wu X, Liu J, Liu X, Wu X, Du Y (2022) Fabrication of carbon doped Cu-based oxides as superior NH_3-SCR catalysts via employing sodium dodecyl sulfonate intercalating CuMgAl-LDH. J Catal 407:265–280. https://doi.org/10.1016/j.jcat.2022.02.004

31. Wang Y, Xie L, Liu F, Ruan W (2019) Effect of preparation methods on the performance of CuFe-SSZ-13 catalysts for selective catalytic reduction of NO_x with NH_3. J Environ Sci 81:195–204. https://doi.org/10.1016/j.jes.2019.01.013

32. Zhao L, Li X, Zhao J (2013) Correlation of structural and chemical characteristics with catalytic performance of hydrotalcite-based CuNiAl mixed oxides for SO_2 abatement. Chem Eng J 223:164–171. https://doi.org/10.1016/j.cej.2013.02.103

33. Lin Q, Feng X, Zhang H, Lin C, Liu S, Xu H, Chen Y (2018) Hydrothermal deactivation over CuFe/BEA for NH_3-SCR. J Ind Eng Chem 65:40–50. https://doi.org/10.1016/j.jiec.2018.04.009

34. Wei F, Liu L, Wu X, Liu J, Wu X (2023) Simultaneous removal of NO_x and toluene on CuMnMgAl layered double oxides (LDO) derived from layered double hydroxides (LDHs) precursor. Catal Lett. https://doi.org/10.1007/s10562-023-04384-1

35. Li X, Li K, Peng Y, Li X, Zhang Y, Wang D, Li J (2018) Interaction of phosphorus with a $FeTiO_x$ catalyst for selective catalytic reduction of NO_x with NH_3: influence on surface acidity and SCR mechanism. Chem Eng J 347:173–183. https://doi.org/10.1016/j.cej.2018.04.035

36. Xu H, Wang Y, Cao Y, Fang Z, Lin T, Gong M, Chen Y (2014) Catalytic performance of acidic zirconium-based composite oxides monolithic catalyst on selective catalytic reduction of NO_x with NH_3. Chem Eng J 240:62–73. https://doi.org/10.1016/j.cej.2013.11.053

37. Gao Q, Ye Q, Han S, Cheng S, Kang T, Dai H (2020) Effect of Ce doping on hydrothermal stability of Cu-SAPO-18 in the selective catalytic reduction of NO with NH_3. Catal Surv Asia 24(2):134–142. https://doi.org/10.1007/s10563-020-09294-5

38. Lin Q, Li J, Ma L, Hao J (2010) Selective catalytic reduction of NO with NH_3 over Mn-Fe/USY under lean burn conditions. Catal Today 151(3–4):251–256. https://doi.org/10.1016/j.cattod.2010.01.026

39. Liu Z, Zhang S, Li J, Ma L (2014) Promoting effect of MoO_3 on the NO_x reduction by NH_3 over CeO_2/TiO_2 catalyst studied with in situ DRIFTS. Appl Catal B 144:90–95. https://doi.org/10.1016/j.apcatb.2013.06.036

40. Wu Z, Jiang B, Liu Y, Wang H, Jin R (2007) DRIFT study of manganese/titania-based catalysts for low-temperature selective catalytic reduction of NO with NH_3. Environ Sci Technol 41(16):5812–5817. https://doi.org/10.1021/es0700350

41. Mei J, Huang W, Qu Z, Hu X, Yan N (2017) Catalytic oxidation of dibromomethane over Ti-modified Co_3O_4 catalysts: structure, activity and mechanism. J Colloid Interface Sci 505:870–883. https://doi.org/10.1016/j.jcis.2017.06.077

42. Gu T, Jin R, Liu Y, Liu H, Weng X, Wu Z (2013) Promoting effect of calcium doping on the performances of MnO_x /TiO_2 catalysts for NO reduction with NH_3 at low temperature. Appl Catal B 129:30–38. https://doi.org/10.1016/j.apcatb.2012.09.003

43. Hua H, Zeng J, Wang G, Zhang J, Zhou J, Pan Y, Xu ZP (2020) Understanding of the high hydrothermal stability of a catalyst prepared from Mn slag for low-temperature selective catalytic reduction of NO. J Hazard Mate. https://doi.org/10.1016/j.jhazmat.2019.120935

44. Liu F, He H, Ding Y, Zhang C (2009) Effect of manganese substitution on the structure and activity of iron titanate catalyst for the selective catalytic reduction of NO with NH_3. Appl Catal B 93(1–2):194–204. https://doi.org/10.1016/j.apcatb.2009.09.029

45. Shu Y, Sun H, Quan X, Chen S (2012) Enhancement of catalytic activity over the iron-modified Ce/TiO_2 catalyst for selective catalytic reduction of NO_x with ammonia. J Phys Chem C 116(48):25319–25327. https://doi.org/10.1021/jp307038q

46. Liu Z, Zhu J, Li J, Ma L, Woo SI (2014) Novel Mn-Ce-Ti mixed-oxide catalyst for the selective catalytic reduction of NO_x with NH_3. ACS Appl Mater Interfaces 6(16):14500–14508. https://doi.org/10.1021/am5038164

47. Chen L, Yuan F, Li Z, Niu X, Zhu Y (2018) Synergistic effect between the redox property and acidity on enhancing the low temperature NH_3-SCR activity for NO_x removal over the $Co_{0.2}Ce_xMn_{0.8-x}Ti_{10}$ (x=0-0.40) oxides catalysts. Chem Eng J 354:393–406. https://doi.org/10.1016/j.cej.2018.07.196

48. Zhang Z, Li R, Wang M, Li Y, Tong Y, Yang P, Zhu Y (2021) Two steps synthesis of $CeTiO_x$ oxides nanotube catalyst: enhanced activity, resistance of SO_2 and H_2O for low temperature NH_3-SCR of NO_x. Appl Catal B. https://doi.org/10.1016/j.apcatb.2020.119542

49. Shi J, Wang Y, Duan R, Gao C, Wang B, He C, Niu C (2019) The synergistic effects between Ce and Cu in $Cu_yCe_{1-y}W_5O_x$ catalysts for enhanced NH_3-SCR of NO_x and SO_2 tolerance. Catal Sci Technol 9(3):718–730. https://doi.org/10.1039/c8cy01949e

50. Ding S, Liu F, Shi X, He H (2016) Promotional effect of Nb additive on the activity and hydrothermal stability for the selective catalytic reduction of NO_x with NH_3 over $CeZrO_x$ catalyst. Appl Catal B 180:766–774. https://doi.org/10.1016/j.apcatb.2015.06.055

51. Li L, Zhang L, Ma K, Zou W, Cao Y, Xiong Y, Dong L (2017) Ultra-low loading of copper modified TiO_2 /CeO_2 catalysts for low-temperature selective catalytic reduction of NO by NH_3. Appl Catal B 207:366–375. https://doi.org/10.1016/j.apcatb.2017.02.041

52. Marban G, Fuertes AB (2002) Kinetics of the low-temperature selective catalytic reduction of NO with NH_3 over activated carbon fiber composite-supported iron oxides. Catal Lett 84(1–2):13–19. https://doi.org/10.1023/A:1021008113948

53. Guo R, Li M, Sun P, Liu S, Wang S, Pan W, Sun X (2017) The enhanced resistance to P species of an Mn-Ti catalyst for selective catalytic reduction of NO_x with NH_3 by the modification with Mo. RSC Adv 7(32):19912–19923. https://doi.org/10.1039/c7ra01876b

54. Liu J, Li X, Zhao Q, Ke J, Xiao H, Lv X, Wang S (2017) Mechanistic investigation of the enhanced NH_3-SCR on cobalt-decorated Ce-Ti mixed oxide: in situ FTIR analysis for structure-activity correlation. Appl Catal B 200:297–308. https://doi.org/10.1016/j.apcatb.2016.07.020

55. Eigenmann F, Maciejewski M, Baiker A (2006) Selective reduction of NO by NH_3 over manganese-cerium mixed oxides: relation between adsorption, redox and catalytic behavior. Appl Catal B 62(3–4):311–318. https://doi.org/10.1016/j.apcatb.2005.08.005

56. Chen L, Li J, Ge M (2010) DRIFT study on cerium-tungsten/titiania catalyst for selective catalytic reduction of NO_x with NH_3. Environ Sci Technol 44(24):9590–9596. https://doi.org/10.1021/es102692b